Proceedings of the 9th IEEE International
Conference on Nano/Micro Engineered and Molecular Systems
April 13-16, 2014, Hawaii, USA

Nanorobotic End-effectors: Design, Fabrication, and *in situ* Characterization

Zheng Fan, *Student Member, IEEE*, Miao Yu, *Student Member, IEEE*, Gautham Dharuman, Xudong Fan, and Lixin Dong, *Senior Member, IEEE*

***Abstract* —This paper reports three types of nanorobotic end-effectors: m@CNTs-based sphere-on-pillar (SOP) optical nanoantennas, nanotube fountain pen, and m@CNTs-based tunneling nanosensor. The fabrication method of the m@CNTs-based SOP optical nanoantennas we developed has potentials in the investigation of nano-optics and nano-photonics due to its feasibility in preparing such devices. Nanotube fountain pen (NFP) illustrates the practical applications in the direct fabrication of nanostructures from 0 to 3D, which is of critical importance in the future fast-prototype of nanodevices. The m@CNTs-based tunneling nanosensor provides a new design in measuring force/displacement in nanoscale, opening a new ground in developing nanoelectromechanical system (NEMS). These three end-effectors enable new functions for the nanorobotic manipulators and extending people's ability in exploring the world in nanoscale.**

***Index Terms* — nanorobotic, end-effector, optical antenna, nanotube fountain pen, nanosensor**

I. Introduction

The pipeline factory that can assemble nano-electromechanical systems (NEMS) is no longer a mere fantasy. Scientists are now attempting to molecularly manufacture nanodevices in a high throughput mode. Richard Feynman predicted 50 years ago that one day people would maneuver things atom by atom by using some sophisticated techniques; today, the nanorobotic manipulator enables the position and manipulation of nanomaterials down to nanoscale or even atomic scale, which largely extends our abilities to explore the "room at the bottom" [1]. With the help of nanorobotic manipulators, researchers have made great progress in several areas such as nanomedicine [2, 3], nano-optics [4], nanophotonics [5], and nanofluidics [6, 7]. Through these investigations, the researchers fabricated and assembled prototype NEMS devices individually by using the manipulator before the large-scale reproduction [8-10]. This resembles the individual manual production mode in the industry's history, which will eventually develop into a large-scale production mode, such as the Fordism production mode. We can imagine an automatic nanomanufacturing pipeline that will one day fabricate nanodevices atom by atom just as robots make cars in assembly-lines. With the advantages of the precise position/displacement control, the nanorobotic manipulator is a perfect "worker" candidate for the future nanomanufacturing pipeline. Unfortunately, no suitable nanotools or nanosensors exist for the reliable nanorobotic batch fabrication nowadays. The conventional end-effectors we use, such as nanoprobes and nanogrippers are too simple to fulfill the requirements of sophisticated nanomanipulation. In order to build a reliable bridge between the nanorobotic manipulator and the nanoworld, the development of the intelligent end-effectors should be tackled first.

In this report we introduce three types of nanorobotic end-effectors, including sphere-on-pillar (SOP) optical nanoantennas, nanotube fountain pen, and m@CNTs-based tunneling nanosensor (Fig. 1).

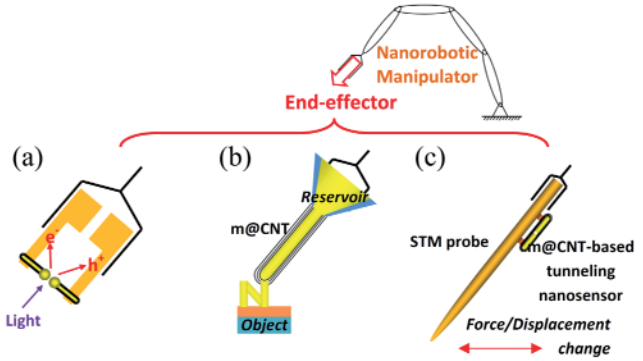

Fig.1 Nanorobotic end-effectors (a) sphere-on-pillar (SOP) optical nanoantennas. (b) nanotube fountain pen. (c) m@CNTs-based tunneling nanosensor.

II. SOP Optical Nanoantennas

We developed the *in situ* fabrication and characterization of the m@CNTs-based optical nanoantennas. By delivering and dwelling the encapsulated metals from m@CNTs onto their tips, the sphere with controllable sizes and shapes can be targeted. Such SOP nanostructures can function as optical antennas for apertureless scanning near-field optical microscopy (SNOM) [11-17], laser trapping [18, 19], or single molecule detection [20, 21] in nanophotonic systems and scanning anodes for field emitters [22] in vacuum nanoelectronic devices.

Z. Fan, M. Yu, G. Dharuman, and L. X. Dong are with the Department of Electrical and Computer Engineering, Michigan State University, East Lansing, MI 48824-1226, USA (phone: 517-353-3918; fax: 517-353-1980; e-mail: ldong@egr.msu.edu).

X. D. Fan is with the Center of Advance Microscopy, Michigan State University, East Lansing, MI 48824-1226, USA.

978-1-4799-4726-3/14/$31.00 © 2014 IEEE

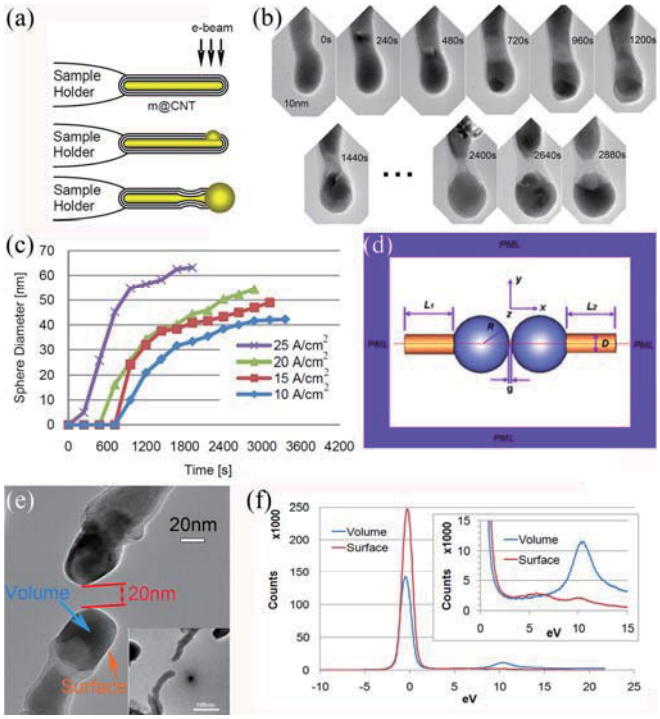

Fig.2 The fabrication and characterization of m@CNTs-based sphere-on-pillar optical nanoantennas (a) The schematic of EBIB. The inner metal of an m@CNT will melt and flow out of the carbon shell due to the exposure of e-beam. (b) Time-resolved EBIB process. A Sn@CNT was brought under the electron beam at t = 0 s. Under the current density of 20 A/cm2 from 240 to 480 s, a molten section of tin appeared and moved to the tip of the tube and the tube tip became more spherical. At t = 720 s, the inner metal first broke out from the tube. After then, metal continues flowing out, and the carbon shell near the tip of the tube deformed severely, which may be responsible to the squeezing out of the sphere from the nanotube shell. At t = 1440 s, a sphere is visible on the tip of CNT and at t = 2880s, the sphere on the tip completed, the shrinkage of the carbon shell prevented the metal flow from the bottom to the top of the tube. (c) Time sequences of bubbling differed at different current densities and tube sizes. (d) A model of a sphere-on-pillar optical nano-antenna. (e) A pair of sphere-on-tip nanostructures fabricated by EBIB. Inset shows a pair of m@CNTs is positioned together before EBIB is performed. (f) EELS excitation on the volume center and the surface of a sphere (Refer to (e) for the positions that the electron beam focused on).

The fabrication processes is named electron-beam-induced bubbling (EBIB). The raw material we used is Sn-filled CNTs (Sn@CNTs). A single-tilt TEM holder is used for EBIB, and a scanning tunneling microscope (STM) built in a TEM holder (FM2000E, Nanofactory Instruments AB) is used as a manipulator. The setup of EBIB is schematically illustrated (Fig. 2(a)). During the EBIB, the current density of the electron beam transmitting through the CNTs is adjusted by changing the focus as well as the magnification, the brightness and the incident area. The final shapes can be either spheres or particles with multiple facets, and are related to the heating and cooling processes. We found that the sizes of the spheres on the tips are related to the exposure time and the orifices of the nanotube. Fig. 2(b) is a series of time-resolved TEM images showing the EBIB process of a Sn@CNT at a current density of 20 A/cm^2 with the magnification of ×300K and the irradiation area of 1.3×10^{-14} cm^2. The accelerating voltage of the electron beam keep at 200 kV in all experiments. By increasing the current density, the local temperature increased due to the increase of the electron energy. Starting from an as-synthesized Sn@CNT, an observable nanosphere formed on the tip of the CNT due to the exposure under the electron beam. At t = 720 s (Fig. 2(b)), the inner molten metal first broke out of the nanotube. In our previous investigations, we observed that the tin nanowire melted entirely in the CNTs when the current density reached 0.4 A/cm^2, and the expansion of the tin wire occurred at the same time [23]. The much higher current density applied here (20 A/cm^2) is attributed to the bubbling of the molten metal. At the beginning of the process, polyhedral nanoparticles (Fig. 2(b), 1200 s) will be formed. Further, it is found that it is possible to convert polyhedral nanoparticles into spheres by increasing the temperature further (Fig. 2(b), 2880 s) [24]. We attribute the bubbling and the shape conversion to the electron irradiation and the secondary effects, including the carbon shell contraction and the surface tension of the molten metal. The encapsulated materials were melted and then squeezed out by the carbon shells as spheres onto the top of nanotubes. Applying an image processing method, the mass of the sphere was analyzed. The CNT has an external diameter of approximately 40 nm. The diameter of the final sphere is 54 nm, and the mass of the resulted sphere is 0.6 fg (femtograms) according to the density of tin (7.31 g/cm^3).

We discovered that the threshold current density for the sphere formation is 20 A/cm^2 with the exposure time of ~720 s. Experiments on several other CNTs showed that the threshold current density varies from 10 to 25 A/cm^2 related to their diameters (37-40 nm). The curves for the bubbling vs. the diameter of the sphere are depicted (Fig. 2(c)), which shows that with the increase of irradiation energy, the starting time for the flowing out is shortened. The starting time varies from 200 to 700 s for the current density from 10 to 25 A/cm^2, and the bubbling time varies from 1900 to 3360s. These variations may be related to the internal temperature and pressure buildup.

According to the experiments, the EBIB process consists of two parts, i.e., the melting of the inner metal and the shrinkage of the carbon shells. The melting was due to the heating of the tin by the irradiation effects as revealed in previous study [23]. The contraction of the carbon shells being observed (Fig. 2(b), 720 to 1440 s) was responsible for the squeezing out of the sphere from the nanotube shell, which resulted from controlled electron beam irradiation on CNTs. The irradiation causes large pressure within the nanotube cores that can deform and extrude the metals from the carbon shells [25]. Therefore, the full process of EBIB is as follows: the rupture of the carbon planes makes defects on the carbon shells, and then the bubbling occurs at these sites. The internal pressure buildup is a result of melting, the thermal expansion of the encapsulated metal, and the shrinkage of the nanotube shells [25]. All of these causes are determined by the current density. As a result, the rates of the nanobubbling and the geometry of the spheres can be controlled by adjusting the current density.

As we proposed in our previous simulation study [13], a pair of such spheres on the pillar nanostructures (Fig. 2(d)) can function as optical antennas. It is known that for plasmonic structures the surface plasmon (SP) resonances strongly depend on the shape and size of the structure as well as the losses from the materials [26]. To justify that the as-fabricated sphere on pillar pairs can function as optical antennas, we completed an experiment using the nanorobotic manipulator holder in the same TEM. Two nanotubes were positioned close to one another (the inset of Fig. 2(e)) and spheres were blown out from them using EBIB. Then, the two spheres were positioned close with a feed gap of 20 nm (Fig. 2(e)). Electron energy loss spectroscopy (EELS) technique was applied for in situ characterization of the resonance performance. The output counts vs. excitation energy (in eV) curves are drawn in Fig. 2(f). It can be seen that the volume plasmon (VP) appears at around 11 eV when the electron probe is placed at the center of the sphere. As the electron probe is placed close to the surface of a sphere, the surface plasmon peak becomes dominant around 6 eV (Fig. 2(f)) (The inset shows the details between 0 - 15 eV). These energy values correspond to the equivalent photons with wavelengths between 113 nm and 226 nm. It is evident that the surface plasmon has a lower energy and thus a larger wavelength, proving that resonance did occur. The m@CNTs-based SOP optical nanoantennas added a new design to the family of optical nanoantennas. Experimentally, this end-effector on a nanorobotic manipulator can be used in nanophotonics investigations more readily than the conventionally near-field optical methods. This is due to the fact that it is easy to use EBIB to fabricate such devices. The manipulator attached with m@CNTs-based optical nanoantennas can be used as SNOM probes, single molecule detectors, and solar cell antennas to enhance energy conversion.

III. Nanotube Fountain Pen

The next end-effector we will introduce is the nanotube fountain pen (NFP). The NFP consists of a reservoir and a nanotube injector to transport metal atoms onto a conductive substrate, forming an arbitrary structure. Complex metal nanostructures from 0D to 3D are realized with a position servo control. The schematic of NFP is illustrated (Fig. 3(a)), where a single Cu@CNT was used as the pen tip and nanotube networks as a reservoir. The STM was used as a nanorobotic manipulator to manually realize the servo control. By positioning the tip on a conductive substrate, a circuit can be established between the two ends of the NFP to achieve mass delivery. The copper inside the neighboring CNTs was sucked into the CNT injector under a stable bias (Fig. 3(b)). It has been estimated from the geometry and the density of copper that the initial mass inside the nanotube injector is 1.9 fg, while the deposited mass is 29.0 fg (about 15 times more than the original mass). The extra mass is attributed to those inside the nanotubes attached to the CNT injector.

The current-time (*I-t*) curve during the continuous mass delivery is shown in Fig. 3(b). As the bias increases from zero in increments of 0.1 V, the delivery begins after the external bias reaches 1.0 V. The initial state (0~300 s)

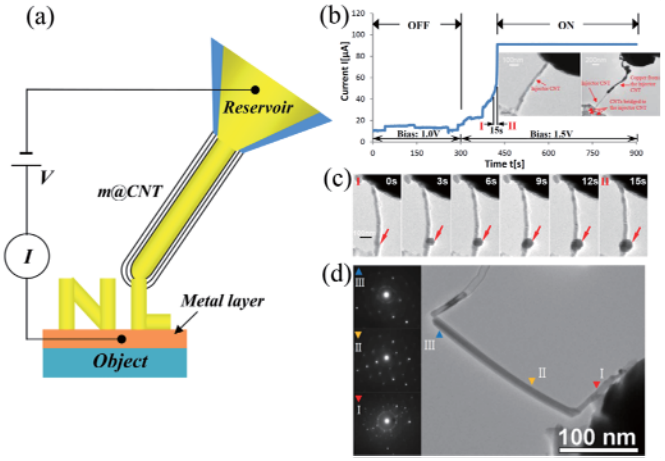

Fig.3 NFP (a) The schematic of NFP. By applying a bias, the encapsulated metal can be continuously flowed out for nanostructure fabrication. (b) *I-t* characterization during the NFP "writing" process. The initial state (0~300) is defined as "OFF" (external bias: 1.0 V) and the state after the mass migration starts as "ON" (external bias: 1.5 V). Insets show the initial mass inside the nanotube injector is 1.9 fg, while the deposited mass is 29.0 fg (about 15 times more than the original mass). (c) Mass accumulation process. The mass is accumulated from the neighbor CNTs. (d) The crystalline phase analysis of as-generated nanowire. Due to the molten state at the connection between the deposit and the injector, it provides possible to shape the deposited structures.

exhibits a normal CNT electrical property, with a conductivity of 30 μS. The degradation process (starting at 300 s) of the resistance occurs as an external bias of 1.5 V is applied. The sudden increase of the current at 410 s is attributed to the healing of the carbon shells under higher voltage bias [27]. In order to prevent the electric breakdown of the nanotube [28, 29], the current is restricted to 90 μA. The accumulation of mass from the reservoir takes place while the current sharply increases. The nanotubes serve as bridges to transfer the mass from the neighboring CNTs to the injector and deposit onto the object [7, 30]. A series of video frames illustrating that the migration begins when the mass was accumulated on the side wall of the tube close to the junction site between the nanotube injector and the network (Fig. 3(c)). A mass of 14 fg was transferred from the external reservoir.

As the nanowires were written on the object, their shape was formed immediately due to the excellent thermal conductivity of the probe that cools down the deposit [31]. Reheating of the cooled-down deposit was not achieved because the volume of the probe (tip radius: 120 nm, root radius: 10 μm) was much larger than that of the copper deposit. The probe served as a heat sink with essentially infinite capacity compared with the copper deposit. A detailed examination of the crystalline structure of the generated nanowire can further explain their shaping process (Fig. 3(d)). At the contact area between the probe and nanotube (area I), the crystalline phase of the deposited copper shows a poly-crystalline phase. This is attributable to

the instant cool-down at the heat sink [31]; the molten mass is not crystallized enough before it forms the solid state. In contrast, area II reveals single-crystalline phases since it is far from the heat sink. Moreover, according to the dark contrast and the amorphous phase seem in area III. We can confirm the molten state at this position. Therefore, the molten state in area III provides opportunity to shape the final structure by manually positioning the injector.

sensing to the manipulator. We attribute this electromechanical coupling effect to inter-nanoparticle tunneling. Since tunneling current scales exponentially with a reduction in inter-nanoparticle separation, the deformation of the nanotube provides a higher order scaling effect of conductivity as a function of strain. This makes tunneling gap embedded m@CNTs as a building block candidate for the application as high resolution NEMS devices.

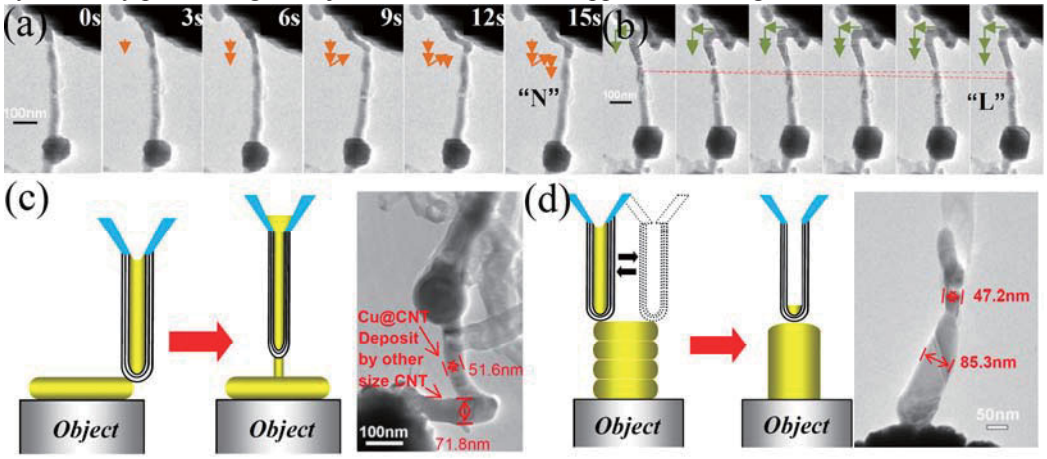

Fig.4 (a) The writing process of the Letter "N". By manually positioning the molten copper onto the probe can freeze it immediately, and thereby construct the nanostructure as depicted a stick figure. (b) The writing process of the Letter "L". (c) The demonstration of using different sized CNTs to generate nanostructures. (d) The demonstration of the modulating of deposits by adjusting the position of injector. The original diameter of nanotube is about 47.2 nm; however, the diameter of deposited nanowire is 85.3 nm, which is much larger than the size of nanotube.

Two 3D capital letters, "N" and "L"; were fabricated. By attaching the tip of the injector to the probe during the mass flow, the shape of the molten nanowire deposit can be adjusted, and the letter "N" will be produced eventually (Fig. 4(a)). For the capital letter "L", the injector was moved during the mass flow to form the letter (Fig. 4(b)). Moreover, it is possible to construct a nanoscale composition with components of different diameters (Fig. 4(c)). Due to the complexity of using nanotubes with different diameters for fabrication, we have also investigated using a single nanotube to fabricate components of different sizes. The representative demonstration (Fig. 4(d)) shows that the injector moved back and forth in a small range, trying to deposit the mass at the same height as much as possible. Hence, those deposits would melt together and form a component that is much larger than the original size of the copper core inside the tube.

As we realized the using of a CNT injector and network as a NFP and illustrated the practical applications of this technique in the direct fabrication of nanostructures from 0 to 3D, we can conclude that the NFP is a promising end-effector to the nanorobotic manipulator, which are of critical importance to the future nanodevices batch fabrication.

IV. M@CNTs-BASED TUNNELING NANOSENSOR

The third end-effector we proposed is a nanoelectromechanical sensor based on an individual tunneling gap embedded m@CNT. As illustrated in the schematic diagram (Fig. 1(c)), this end-effector demonstrates its potential use for both position and force

The quantitatively understand the tunneling effect in a peapod nanostructure, we modeling the relation between the inter-particle spacing and the tunneling current. The metal-insulator-metal (MIM) model is applied here, the approximate expression for the tunneling current is given by [32]:

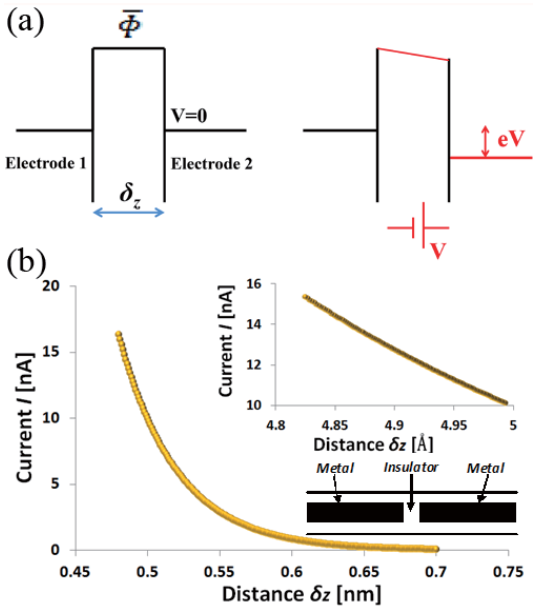

Fig.5 (a) The schematic of the inter-nanoparticle tunneling without external bias and with the bias voltage. (b) The tunneling current in a nanowire based MIM system.

$$I = \frac{eS}{2\pi\bar{h}\delta_z{}^2}\left[\bar{\Phi}e^{-\frac{\sqrt{8m}}{\bar{h}}\delta_z\sqrt{\bar{\Phi}}} - (\bar{\Phi}+eV)e^{-\frac{\sqrt{8m}}{\bar{h}}\delta_z\sqrt{\bar{\Phi}+eV}}\right] \quad (1)$$

as shown in the schematic of the inter-nanoparticle tunneling (Fig. 5(a)), where S is the contact area, δ_z is the inter-particle separation, $\bar{\Phi}$ is the average barrier height between the two electrodes, m is the mass of the electron, $\bar{h}$ is the *Plank constant*, and V is the voltage between the electrodes. Here we assume the average barrier height $\bar{\Phi}$ = 5 eV, then the Current-Distance (I-δ_z) relation can be achieved (Fig. 5(b)). As shown in the demonstrated tunneling current curve, the increasing of the current scales exponentially to the decrease of the distance (as the distance between two electrodes decrease from 6.5 Å to 0.5 Å, the tunneling current increase from 0.25 nA to 10 nA, 40 times larger than the original current), which highly suggests a novel sensing mechanism.

However, since now, there are no methods exist for reliably preparing a peapod nanostructure. This lack of control has been seen as the primary block for the realization of this nanotube-based sensor. Here we propose a gap fabrication process by using the nanorobotic mass transport, which enables us to manipulate the mass transport inside the tube with the thermal migration effect and the electromigration effect [33]. The setup of the experiment is similar to the NFP writing process (Fig. 6(a)), we also use Cu@CNT as starting material. When the external bias reaches 2.0 V (0 s) (Fig. 6(a)), the dark contrast and the boiling sign indicate the molten state of the copper wire. As we slowing down the bias increasing speed by decreasing the increments to 0.05 mV, the gradual mass migration could be observed more clearly. As the voltage is increased to 2.2 V (7 s), the mass in the center suddenly evaporates, revealing the thermal effect that evaporates the mass in the hottest center area [27]. Nevertheless, by further increasing the voltage to 2.5 V (11 s), the electromigration force will reinforce and overcomes the thermal force, which dominates the mass flow from cathode to anode in a singular direction. We carried out the same experiment on a nanotube attached with a reservoir, the process is similar to the previous one; initially, the mass in the center evaporates and then flows from the anode to the cathode. The relation between the transferred mass and time inside the tube is given as: $m = 0.0168t^2 - 0.0681t + 1.9971$ (Fig. 6(b)). Thus, the flow rate is expressed as: $dm/dt = 0.0336t - 0.0681$, indicating a linear mass flow. When the reservoir is attached on the bottom, the mass from the reservoir could linearly migrate into the nanotube and fill up gap between the upper and lower portion. As we detached the electrode contact or suddenly decrease the bias into 0 V, the mass migration will terminate and forms a gap between the two parts of copper mass. Since the mass migration inside the tube is linear, the gap distance is able to be controlled. Then we can limit the gap distance down to around 1 nm (Fig. 6(c)).

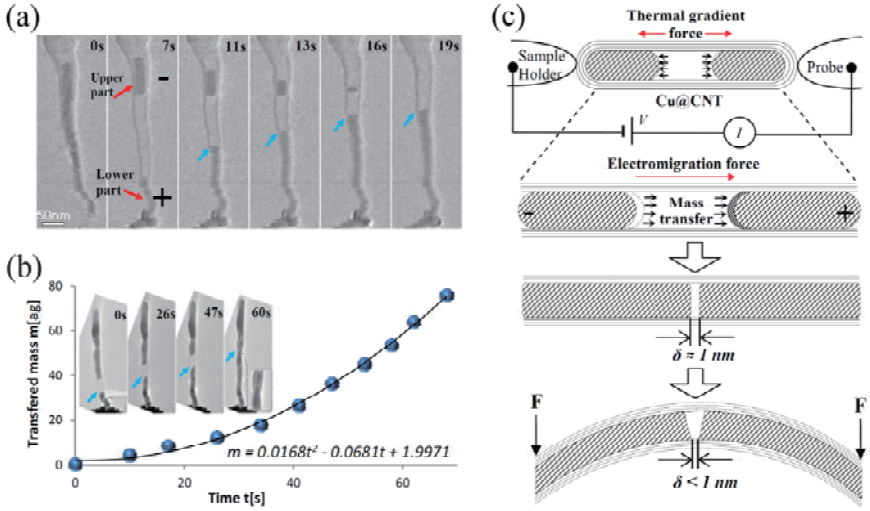

Fig.6 (a) The process shows the electromigration force and thermal gradient force during the mass transportation process. When the bias reached 2.2 V, the inner mass was separated in the center and transferred to the two ends, formed a "gap". As the center of the nanotube was presumed to be the high-resistance point, or "hottest spot," the thermal gradient force in turn diverted from the center towards the two ends; therefore, the inner mass split process is obviously attributed to the actuation of temperature gradient force. By further adding the voltage at 0.1 V intervals until the external bias reached 2.5 V, it can be noted that with the reinforcement of electromigration effect, the mass is transferred from the upper part to the lower part in an average rate of 2.2 ag/s. (b) The mass flow rate study on a Cu@CNT combined with a network reservoir. The relation between the transferred mass and time inside the tube was given as: $m = 0.0168t^2 - 0.0681t + 1.9971$. Thus, the flow rate was expressed as: dm/dt = 0.0336t - 0.0681, indicate a linearly accessed mass flow. (c) The process of generating a tunnelling gap by mass transport.

In this work, the m@CNT with a tunneling gap structure has been fabricated exhibits a unique tunneling behavior that is a function of material buckling deformation. As we bend the nanotube by using the manipulator, both the nanotube and the inner copper will deform and the inner gap spacing will decrease down to subnanometer range (Fig. 6(c)). Due to the tunneling in this range when we apply the bias, current density j_t scales with inter-nanoparticle separation exponentially, $j_t \sim e^{-\delta}$. This exponential increase can further amplify the strain-induced resistance change, and can provide extremely high sensitivity.

V. Conclusions

In summary, we have experimentally investigated three types of end-effectors that are based on m@CNTs: m@CNTs-based SOP optical antennas, nanotube fountain pen, and m@CNT-based tunneling nanosensor. The efforts to develop these novel end-effectors will open new possibilities in micro-nanoelectromechanical systems (MEMS/NEMS), creating additional functions for nanorobotics and further extending our ability to explore the world in nanoscale.

Acknowledgement

This work is supported by the NSF (IIS-1054585)

References

[1] R. P. Feynman, "There's plenty of room at the bottom," *Caltech's Engineering and Science,* vol. 23, no. 5, pp. 22-36, 1960.

[2] S. Martel, O. Felfoul, J. B. Mathieu, A. Chanu, S. Tamaz, M. Mohammadi, M. Mankiewicz, and N. Tabatabaei, "Mri-based medical nanorobotic platform for the control of magnetic nanoparticles and flagellated bacteria for target interventions in human capillaries," *International Journal of Robotics Research,* vol. 28, no. 9, pp. 1169-1182, Sep 2009.

[3] R. A. Freitas, *Nanomedicine, volume i: Basic capabilities*: Landes Bioscience Georgetown, TX, 1999.

[4] M. Ohtsu and H. Hori, *Near-field nano-optics: From basic principles to nano-fabrication and nano-photonics*: Plenum Publishing Corporation, 1999.

[5] O. Benson, "Assembly of hybrid photonic architectures from nanophotonic constituents," *Nature,* vol. 480, no. 7376, pp. 193-199, Dec 2011.

[6] L. X. Dong, X. Y. Tao, L. Zhang, X. B. Zhang, and B. J. Nelson, "Nanorobotic spot welding: Controlled metal deposition with attogram precision from copper-filled carbon nanotubes," *Nano Letters,* vol. 7, no. 1, pp. 58-63, Jan 2007.

[7] L. X. Dong, X. Y. Tao, M. Hamdi, L. Zhang, X. B. Zhang, A. Ferreira, and B. J. Nelson, "Nanotube fluidic junctions: Internanotube attogram mass transport through walls," *Nano Letters,* vol. 9, no. 1, pp. 210-214, Jan 2009.

[8] J. A. Weldon, B. Aleman, A. Sussman, W. Gannett, and A. K. Zettl, "Sustained mechanical self-oscillations in carbon nanotubes," *Nano Letters,* vol. 10, no. 5, pp. 1728-1733, May 2010.

[9] G. E. Begtrup, W. Gannett, T. D. Yuzvinsky, V. H. Crespi, and A. Zettl, "Nanoscale reversible mass transport for archival memory," *Nano Letters,* vol. 9, no. 5, pp. 1835-1838, 2009.

[10] Y. H. Gao, Y. Bando, Z. W. Liu, D. Golberg, and H. Nakanishi, "Temperature measurement using a gallium-filled carbon nanotube nanothermometer," *Applied Physics Letters,* vol. 83, no. 14, pp. 2913-2915, Oct 2003.

[11] L. Novotny, "Nano-optics - optical antennas tuned to pitch," *Nature,* vol. 455, no. 7215, p. 887, Oct 2008.

[12] P. Muhlschlegel, H. J. Eisler, O. J. F. Martin, B. Hecht, and D. W. Pohl, "Resonant optical antennas," *Science,* vol. 308, no. 5728, pp. 1607-1609, Jun 2005.

[13] X. D. Cui, L. X. Dong, W. H. Zhang, W. Wu, Y. Tang, and D. Erni, "Numerical investigations of a multi-walled carbon nanotube-based multi-segmented optical antenna," *Applied Physics B: Lasers and Optics,* vol. 101, no. 3, pp. 601-609, Nov. 2010.

[14] A. M. Kern and O. J. F. Martin, "Excitation and reemission of molecules near realistic plasmonic nanostructures," *Nano Letters,* vol. 11, no. 2, pp. 482-487, Feb 2011.

[15] P. Bharadwaj and L. Novotny, "Robustness of quantum dot power-law blinking," *Nano Letters,* vol. 11, no. 5, pp. 2137-2141, May 2011.

[16] T. Kalkbrenner, U. Hakanson, A. Schadle, S. Burger, C. Henkel, and V. Sandoghdar, "Optical microscopy via spectral modifications of a nanoantenna," *Physical Review Letters,* vol. 95, no. 20, art. no. 200801, Nov 2005.

[17] M. Fleischer, A. Weber-Bargioni, M. V. P. Altoe, A. M. Schwartzberg, P. J. Schuck, S. Cabrini, and D. P. Kern, "Gold nanocone near-field scanning optical microscopy probes," *ACS Nano,* vol. 5, no. 4, pp. 2570-2579, Apr 2011.

[18] M. Righini, P. Ghenuche, S. Cherukulappurath, V. Myroshnychenko, F. J. G. de Abajo, and R. Quidant, "Nano-optical trapping of rayleigh particles and escherichia coli bacteria with resonant optical antennas," *Nano Letters,* vol. 9, no. 10, pp. 3387-3391, Oct 2009.

[19] M. L. Juan, M. Righini, and R. Quidant, "Plasmon nano-optical tweezers," *Nature Photonics,* vol. 5, no. 6, pp. 349-356, Jun 2011.

[20] P. Anger, P. Bharadwaj, and L. Novotny, "Enhancement and quenching of single-molecule fluorescence," *Physical Review Letters,* vol. 96, no. 11, art. no. 113002, Mar 2006.

[21] C. Hoppener and L. Novotny, "Antenna-based optical imaging of single ca^{2+} transmembrane proteins in liquids," *Nano Letters,* vol. 8, no. 2, pp. 642-646, Feb 2008.

[22] L. X. Dong, A. Subramanian, D. Hugentobler, B. J. Nelson, and Y. Sun, "Nano encoders based on vertical arrays of individual carbon nanotubes," *Advanced Robotics,* vol. 20, no. 11, pp. 1281–1301, Nov. 2006.

[23] X. Y. Tao, L. X. Dong, W. K. Zhang, X. B. Zhang, J. P. Cheng, H. Huang, and Y. P. Gan, "Controllable melting and flow of β-sn in flexible amorphous carbon nanotubes," *Carbon,* vol. 47, no. 13, pp. 3122-3127, Nov. 2009.

[24] X. D. Feng, D. C. Sayle, Z. L. Wang, M. S. Paras, B. Santora, A. C. Sutorik, T. X. T. Sayle, Y. Yang, Y. Ding, X. D. Wang, and Y. S. Her, "Converting ceria polyhedral nanoparticles into single-crystal nanospheres," *Science,* vol. 312, no. 5779, pp. 1504-1508, Jun 2006.

[25] L. Sun, F. Banhart, A. V. Krasheninnikov, J. A. Rodriguez-Manzo, M. Terrones, and P. M. Ajayan, "Carbon nanotubes as high-pressure cylinders and nanoextruders," *Science,* vol. 312, no. 5777, pp. 1199-1202, May 2006.

[26] J. Rybczynski, K. Kempa, Y. Wang, Z. F. Ren, J. B. Carlson, B. R. Kimball, and G. Benham, "Visible light diffraction studies on periodically aligned arrays of carbon nanotubes: Experimental and theoretical comparison," *Applied Physics Letters,* vol. 88, no. 20, art. no. 203122, May 2006.

[27] X. Y. Huang, Z. Y. Zhang, Y. Liu, and L. M. Peng, "Analytical analysis of heat conduction in a suspended one-dimensional object," *Applied Physics Letters,* vol. 95, no. 14, art. no. 143109, Oct 2009.

[28] P. C. Collins, M. S. Arnold, and P. Avouris, "Engineering carbon nanotubes and nanotube circuits using electrical breakdown," *Science,* vol. 292, no. 5517, pp. 706-709, 2001.

[29] J. Y. Huang, S. Chen, S. H. Jo, Z. Wang, D. X. Han, G. Chen, M. S. Dresselhaus, and Z. F. Ren, "Atomic-scale imaging of wall-by-wall breakdown and concurrent transport measurements in multiwall carbon nanotubes," *Physical Review Letters,* vol. 94, no. 23, art. no. 236802, Jun 2005.

[30] L. X. Dong, X. Y. Tao, L. Zhang, X. Zhang, and B. Nelson, "Plumbing the depths of the nanometer scale," *Nanotechnology Magazine, IEEE,* vol. 4, no. 1, pp. 13-22, 2010.

[31] Z. Fan, X. Y. Tao, X. D. Cui, X. D. Fan, X. B. Zhang, and L. X. Dong, "Shaping the nanostructures from electromigration-based deposition," in *Proc. of the 2010 IEEE Nanotechnology Materials and Devices Conference (IEEE-NMDC2010)*, Monterey, California, 2010, Oct. 12-15, pp. 22-25.

[32] J. G. Simmons, "Generalized formula for electric tunnel effect between similar electrodes separated by a thin insulating film " *Journal of Applied Physics,* vol. 34, no. 6, pp. 1793-1803, 1963.

[33] Z. Fan, X. Tao, X. Zhang, and L. Dong, "Nanorobotic mass transport," in *Nanotechnology (IEEE-NANO), 2012 12th IEEE Conference on*, 2012, pp. 1-4.